The Journal of Adhesion, 85:736–754, 2009

ISSN: 0021-8464 print/1545-5823 online
DOI: 10.1080/00218460902997232

Taylor & Francis
Taylor & Francis Group

Fracture in Composite/Aluminium Joints of Variable Adhesive Properties

M. Budzik[1,2], J. Jumel[1], K. Imielińska[2], and M. E. R. Shanahan[1]
[1]Université Bordeaux 1, Laboratoire de Mécanique Physique (LMP) UMR CNRS 5469, Talence, France
[2]Technical University of Gdansk, Faculty of Mechanical Engineering, Department of Material Science and Engineering, Gdansk, Poland

A strain gauge technique recently developed with the wedge test, for estimating crack length and, thus, the fracture energy of structural adhesive bonding, has been employed on a system in which one adherend had two types of surface treatment. Simple polishing and polishing with subsequent sandblasting were the treatments used, with a distinct straight line, perpendicular to the sample edges, separating the two. Despite the clear-cut difference in surface treatment, smooth transitions in crack growth speed were noted. This can be explained by the existence of a curved crack front, encroaching gradually on one surface-treated zone, whilst remaining partially on the other. Crack length, a*, vs. time,* t*, curves were exploited to obtain fracture energy* vs. *crack speed. The multi-valued nature of the relation can also be explained by a non-rectilinear fracture front. The method is proposed as a method for reproducible comparison of surface treatments.*

Keywords: Adhesive bond failure; Crack length; Fracture; Strain gauges; Surface treatment; Wedge test

INTRODUCTION

Fracture mechanics analysis is much used to assess the initial strength of structural adhesive joints, their durability, and the usefulness, or efficiency, of surface treatments prior to bonding. Various adhesion tests are available for evaluating the fracture strength, G_c, including the double cantilever beam (DCB) and its close relative,

Received 15 December 2008; in final form 29 March 2009.
Address correspondence to M. E. R. Shanahan, Université Bordeaux 1, Laboratoire de Mécanique Physique, 351 Cours de la Libération, F-33405 Talence Cédex, France. E-mail: m.shanahan@lmp.u-bordeaux1.fr

the (so-called Boeing) wedge test. These tests are amongst those giving the most reliable information about fracture energy [*e.g.*, 1–6]. Provided care is taken in choosing joint and test dimensions, bond separation can be attained without leading to excessive (irreversible, plastic) adherend strain near the fracture front [6,7], thus facilitating evaluation of adhesive properties.

The basic technique in both the wedge test and the DCB is to force a bonded joint open, perpendicularly to the bond plane, and thus in mode 1, in fracture mechanics nomenclature. However, differences in method of load application differentiate the two. The DCB is usually used at imposed *rate of* separation, whereas the wedge test employs imposed separation (*distance*, hence the term wedge, used for keeping two adherends apart at one end of the joint). (The DCB also tends to be used with thicker adherends.) In the wedge test, the two adherends are bonded along their length, except at one extremity, wherein a wedge is inserted, in order to force debonding [2]. An advantage is that the test is "autonomous," in that, once the wedge is in place, no further interference is required, except for measuring crack length, a, as a function of time, t. Crack growth is "driven" by the restitution of stored, elastic, strain energy stored in the bent adherends, mainly from the wedge up to the crack front [8]. In addition, fracture energy, G_c, follows a scaling rule of the form $G_c \sim a^{-4}$, ensuring stability of crack growth [9,10]. Crack length measurement is, however, not always simple, and precision is needed.

With this in mind, the present authors recently presented a strain gauge method for the continuous and accurate evaluation of crack length [11]. By combining the data from various strain gauges in their different relative positions with respect to the crack front, an accurate, and potentially continuous assessment of crack length can be obtained. The technique of attaching strain gauges to the "back face" of an adherend has also been used with various other joint geometries [12–17].

In the present contribution, we extend use of the strain gauge method developed in order to investigate crack growth behaviour in the case of variable adherend surface pretreatment. The basic idea is to alter the surface treatment of one and the same adherend, but in separate zones, prior to bonding, with a knowledge that one treatment is likely to produce markedly better adhesion than the other. Simple measurement of the fracture energy on each surface is relatively easy and should hold no surprises. Nevertheless, the fact that it is *possible* to vary surface pretreatment on one and the same adherend could prove useful in order to obtain more reliable comparative data on the quality of adhesion of different surface preparations and/or aging conditions, eliminating, or at least reducing, experimental scatter due to the use

of separate joints (individual, slightly different adherends, reproducibility of curing temperature and pressure, etc.).

However, our principal aim here is to consider crack behaviour near the transition from one surface pretreatment to another. Some initially surprising results are obtained which can be successfully explained by invoking the curvilinear nature of the crack front.

EXPERIMENTAL

Materials

In this study, the basic wedge test used was asymmetric and applied to a composite material bonded to an aluminium plate. The epoxy composite was made of six layers of orthogonal pre-preg HexPly® M10/42%/193P/CHS-3k/1000 mm (Hexcel, Stamford, CT, USA), leading to a thickness, h, of 1.22 mm after curing at 120°C under 0.3 bar pressure for 1 hour. Young's modulus, E_C, obtained from 3-point bending, was evaluated at 50 ± 5 GPa, and Poisson's ratio, ν_C, obtained by ultra-sound, was 0.05. (These values lead to a flexural rigidity, $D = E_C h^3/[12(1-\nu_C^2)]$, of *ca*. 7.6 Nm.) The aluminium plate was of Dural® AA 2024 (Alcoa, Pittsburgh, PA, USA) of 5 mm thickness, with a Young's modulus, E_A, of *ca*. 70 GPa and a Poisson's ratio, ν_A, of *ca*. 0.33. These represented, respectively, the "flexible," or thin, and the "rigid," or thick, adherends. Relative flexural rigidity is governed by the ratio of the cubes of thickness multiplied by the appropriate Young's modulus, thus giving a figure of $h_A^3 E_A/(h_C^3 E_C)$ of *ca*. 95, where suffixes A and C refer to aluminium and composite. The terms rigid and flexible are, therefore, reasonable.

Adherends of length 150 mm and width, b, of 25 mm were bonded along 105 mm, as shown in Fig. 1. (The basic geometry is similar to the test ASTM D 3762, the main difference being that the present test is asymmetric.) Two strain gauges (see below) were attached to the outer surface of the flexible, composite plate, along the centre line and in the positions shown. The figure suggests that one strain gauge initiates *within* the bonded length of the assembly, but, in practice, the adhesive bond was pre-cracked from the wedge end, so both gauges were effectively in the de-bonded section. The adhesive used was a commercial epoxy resin (Bostik, La Défense, Paris, France) consisting of bisphenol A of average molecular weight <700 cured with N (3 dimethylaminopropyl) – 1, 3 propylenediamine. Crosslinking was effected at ambient temperature (*ca*. 20°C) for 48 hours under 0.3 bar pressure and at *ca*. 55% RH. PTFE inserts (spacers) were added to prevent bonding at the joint extremities. Bondline thickness

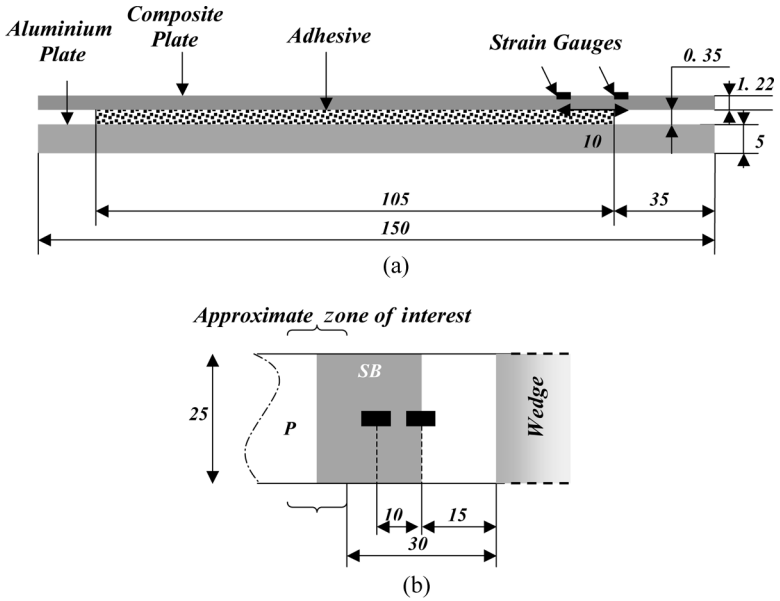

FIGURE 1 Geometry of asymmetric wedge test sample with strain gauges (dimensions in mm). (a) Side view and (b) close-up top view showing the relative position of the wedge and one of the zones of sandblasting.

was maintained at $350 \pm 25\,\mu m$ (measured by optical microscopy) by inserting PTFE spacers at the two point extremities before crosslinking. The constancy was checked by optical microscopy.

Two different surface treatments of the aluminium were used prior to bonding. In both cases, the aluminium to be bonded was lightly abraded with 1200 grade emery paper, followed by surface degreasing with detergent solution, drying in hot air, and rinsing in acetone. This was the only treatment for parts of the surface, and is represented by *P* (polishing). These parts were then carefully protected with adhesive tape, and the remaining surface to be bonded was sandblasted, using SiO_2 grit of average diameter $9\,\mu m$. We refer to these zones as *SB* in the following.

After removing the tape, both composite and aluminium were lightly rinsed with C_2H_5OH before bonding.

Asymmetric Wedge Test

The technique used to estimate crack length, a, depends on strain measurements obtained from gauges bonded to the "bent beam", corresponding to the separated section of the adhesive joint, and as

described in [11]. With the present geometry, effects of bending in the aluminium beam are negligible.

As shown in Fig. 1, two longitudinal strain gauges (Vishay Micro-Measurements, reference EA-13–060LZ-120/E, of nominal resistance 120 Ω, Vishay, Malvern, PA, USA) were fixed to the upper, exposed, side of the flexible adherend, along the centre line, and at distances x_1 and x_2 from the origin, corresponding to wedge/strain gauge distances along the crack propagation axis. The values of x_1 and x_2 were, respectively, 15 and 25 mm. An aluminium wedge of thickness, Δ, of 3 mm was inserted manually to the required depth, corresponding to the origin of x. Joint failure by progressive crack growth at, or near, the bondline was allowed to take place without further interference. Strain gauge recordings were made continuously using a Wheatstone bridge arrangement (Vishay Micromesures 2100 System Multi Channel Signal Conditioner/Amplifier with five modules of Model 2120 B Strain Gauge Conditioner/Amplifier, and one module of Model 2110 B Power Supply). Values of strain thus evaluated correspond to (negative) surface strains at $h/2$ from the adherend neutral surface, and at the values of x_1 and x_2 given above. The main region of interest in this study is the transition between *SB* and *P* surface treatments, as depicted schematically in Fig. 1(b).

Tests reported here were based on two separate assemblies, results being found reproducible. Experiments were effected at $20 \pm 2^{\circ}$C and at an ambient humidity of *ca.* 55% RH.

RESULTS AND DISCUSSION

Fracture Surfaces

The first results presented are a visual assessment of fracture surfaces, which is shown in Figs. 2 and 3. Figure 2 corresponds to a photograph of the side view, [as in Fig. 1(a)] of a composite/aluminium joint after fracture, in the vicinity of the transition zone from *SB* to *P* treatment. The crack proceeded from the right towards the left in the photograph. It is clearly visible that the fracture surface changes radically at the frontier between the two surface treatments. The thin band between the composite and the aluminium is the adhesive layer, which adheres to the latter when *SB* treated, separation occurring at, or near, the adhesive/composite interface (see below). However, when the fracture front enters the region of *P* surface treatment, there is a relatively rapid deviation of crack path, with separation occurring at, or near, the adhesive/aluminium interface. This suggests strongly that the *SB*-treated aluminium presents better adhesion to the

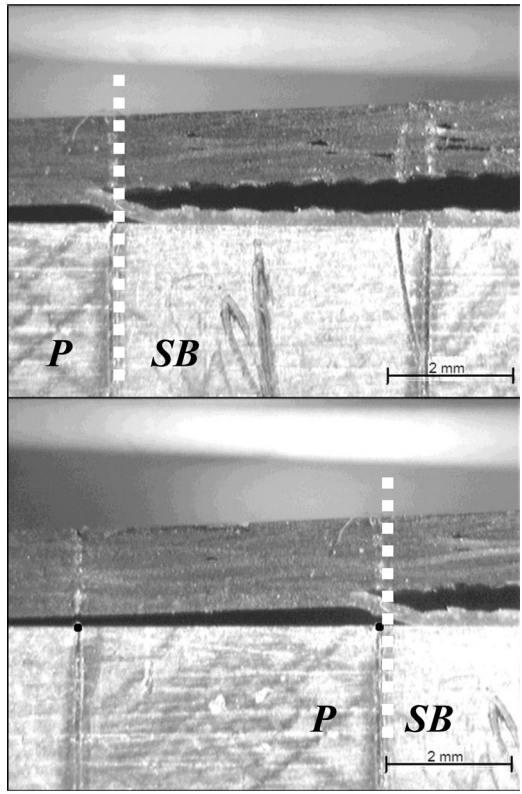

FIGURE 2 Photographs of side of fractured composite (top)/aluminium (bottom) joint in the vicinity of the transition zone between sandblasted (*SB*) and polished (*P*) surfaces. The fracture front comes from the right. The vertical dotted lines represent the position of the transition of surface treatment.

adhesive than does the composite, but that the *P* surface has poorer adhesion. This may be expected from the nature of the surface treatments, but corroboration from energetic considerations follows below, in the context of a description of the transition behaviour.

Figure 3 shows details (pictured from the side) of the fracture zone near the *SB*-treated aluminium, obtained by scanning electron microscopy (SEM). It is clear that the macroscopically interfacial failure at the adhesive/composite interface is, in fact, a cohesive failure within the adhesive, but near the interface. This weakness in the interfacial region, or *interphase*, was first proposed by Bikerman in the context of a weak boundary layer (WBL) [18], and later discussed by Sharpe and Maguire *et al.* [19,20]. It is also clear that the adhesive/aluminium

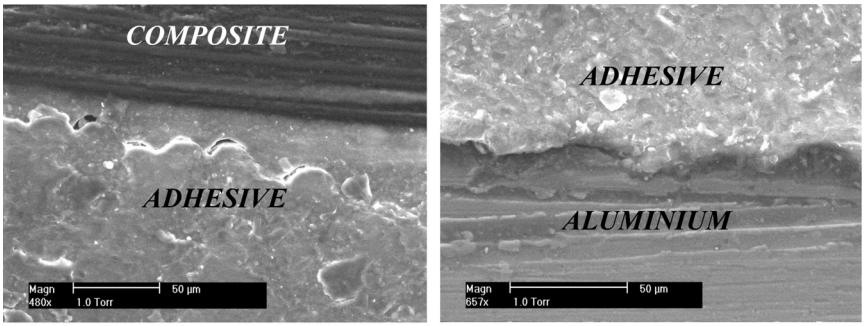

(a) (b)

FIGURE 3 SEM photomicrographs of the side of surfaces near the fracture zone in the *SB* treated region. (a) The macroscopically interfacial failure at the adhesive composite interface is in fact a cohesive failure within the adhesive, but near the interface, whereas (b) the adhesive/aluminium interface remains intact.

interface (interphase?) remains intact when the latter has received the *SB* treatment.

Interpretation of Strain Gauge Measurements

Before going further in analysis of the results, it is useful to recall that the basic principle of the technique employed here is to assess crack length, a, as a function of time, t, and then evaluate fracture energy, G_c, from a and material (Young's modulus of the composite, E_C) and geometrical (composite, h, and wedge, Δ, thickness) parameters. Fracture energy is then considered as a function of fracture rate (da/dt) and aluminium surface treatment. The main difficulty is in the successful, and precise, determination of crack length. In a previous article, we presented a strain gauge technique capable of achieving this goal successfully [11]. It is here exploited, in slightly simplified form, in order to study the adhesion along a wedge type joint presenting different surface treatments. We give a summary below of the analysis detailed in Reference [11].

Referring to Fig. 4 and using the Cartesian coordinates shown, (x,z), ignoring any dependence on width coordinate y (to be introduced later), the displacement perpendicular to the interface of (the central surface of) the flexible adherend, z(x), can be shown by simple beam theory to be given by:

$$z(x) = \frac{\Delta}{2}\left[\left(\frac{x}{a}\right)^3 - 3\left(\frac{x}{a}\right) + 2\right]. \quad (1)$$

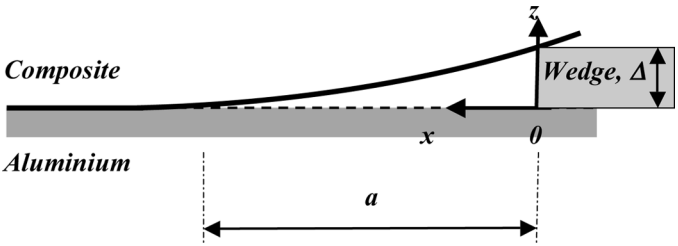

FIGURE 4 Sketch of geometry of asymmetric composite/aluminium wedge test with nomenclature used.

Local curvature, R^{-1}(x), is given approximately by $R^{-1}(x) \approx z_{xx}(x) \approx 3\Delta x/a^3$ and since (outer) surface strain, $\varepsilon_s(x) = \varepsilon(x, h/2) = -h/2R(x)$, where h is composite thickness, we have:

$$|\varepsilon_s(x)| = \frac{3\Delta h x}{2a^3}. \tag{2}$$

Note that we use the absolute value, $|\varepsilon_s\ (x)|$, since $\varepsilon_s(x)$ is, in fact, negative. There is, thus, a linear relationship between $|\varepsilon_s\ (x)|$ and x, the distance between strain gauge (centre) and inserted wedge for a given crack length, a. It is possible, in principle, to ascertain a and its evolution with time, t, $a(t)$, from Eq. (2) and measurements of $|\varepsilon_s(x, t)|$, with a knowledge of Δ, h, and a *single* value of x from the geometry of the joint, with the proviso that the value of x in question is in the unbonded section of the adherend and greater than 0. In the earlier study [11], we employed several strain gauges (4 or 5, depending on the case) but here we use two strain gauges with their centres at 15 and 25 mm from the wedge extremity.

Using the linear relationship between $|\varepsilon_s\ (x, t)|$ and x, *viz*. Eq. (2), in Reference [11] a statistical treatment was presented to allow the optimal use of the 4 (or 5) simultaneous strain gauge readings. Here, we employ only two strain gauges, but with the regression line linking $|\varepsilon_s\ (x)|$ to x being "forced" *via* the origin; this effectively constitutes a third pair of values. (There is no bending moment applied to the beam at the origin of x, only a force.) The statistical treatment leads to an expression for the gradient of Eq. (2):

$$\alpha = \frac{\sum_{i=1}^{n} x_i \varepsilon_i}{\sum_{i=1}^{n} x_i^2}, \tag{3}$$

where $\alpha(t) = 3\Delta h/(2a^3(t))$, Δ being wedge thickness, h representing flexible adherend thickness, and t denoting time dependence of a, and therefore α. The term ε_{i} is short for $|\varepsilon_s\,(x)|$, with an index i. The associated estimated error is given by:

$$\Delta\alpha = \frac{s_n(\varepsilon)}{\left(\sum_{i=1}^{n} x_i^2\right)^{1/2}} = \frac{\left\{\sum_{i=1}^{n} \varepsilon_i^2 - \left(\sum_{i=1}^{n} x_i\varepsilon_i\right)^2 \Big/ \sum_{i=1}^{n} x_i^2\right\}^{1/2}}{(n-1)^{1/2}\left(\sum_{i=1}^{n} x_i^2\right)^{1/2}}, \qquad (4)$$

where $s_n\,(\varepsilon)$ is the best estimate of the standard deviation of ε.

In this elementary analysis, any potential effects of elastic foundation have been neglected [8,10,21,22].

Note that Young's modulus of the flexible beam is not required, provided that both it and the beam cross-section remain constant.

Crack Length and Fracture Energy

Using the strain gauge technique described above, evaluation of crack propagation kinetics can be made virtually continuously, leading to detailed crack monitoring. An example of this is clearly shown below. Figure 5 represents an example of crack length, *a, vs* time, *t*, for the

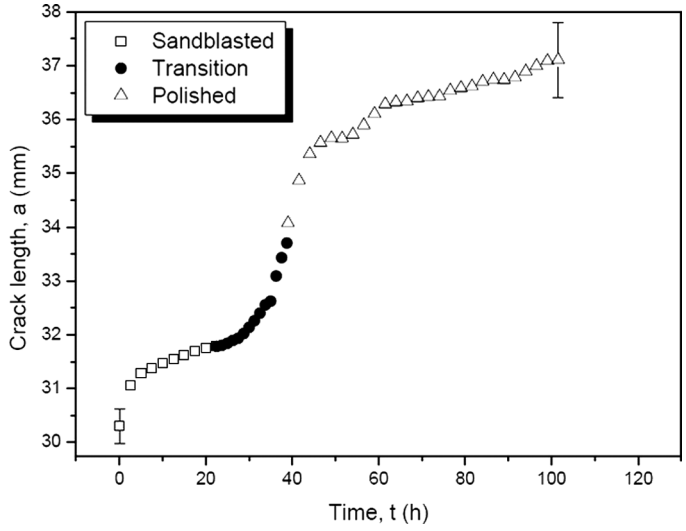

FIGURE 5 Crack length, *a, vs* time, *t*, for the composite/aluminium assembly in the vicinity of the transition from *SB* to *P* surface treatment. The transition is occurring between *ca*. 20 and 40 hours.

composite/aluminium assembly whilst the fracture is occurring in the vicinity of the SB/P transition. Crack length was ascertained as described above, and the two representative error bars on a, at 0 and 100 hours, correspond to the combination of Eq. (4) with estimated errors in h and Δ (each 0.02 mm), by standard propagation of error theory [11]. Intermediate values of a have intermediate estimated errors. However, these allow for *systematic* errors on a occurring due to possible misestimates of h and Δ. More important are *relative* errors on a, the Δa given by standard treatment of Δa from Eq. (4). These are negligible, being of the order of the width of the symbol representing experimental values.

It is usual in wedge tests to observe an asymptotically decreasing crack speed, da/dt. This is due to a constantly decreasing (strain) energy release rate, G. However, Fig. 5 presents three distinctive sections: from $t = 0$ to *ca*. 20 hours, the usual decrease in da/dt is observed, and then from *ca*. 20 to *ca*. 40 hours, crack growth accelerates. Finally, from *ca*. 40 hours onwards, da/dt decreases again, albeit with a couple of minor oscillations.

These results are perhaps more clear when presented as da/dt *vs*. t., as shown in Fig. 6. The initial high crack speed near $t = 0$, due to a relatively high value of G in the early stages of fracture, becomes attenuated, only to pick up again from *ca*. 20 hours, with a peak of *ca*. 0.6 mm/h near $t = 40$ hours. Thereafter, the crack speed again

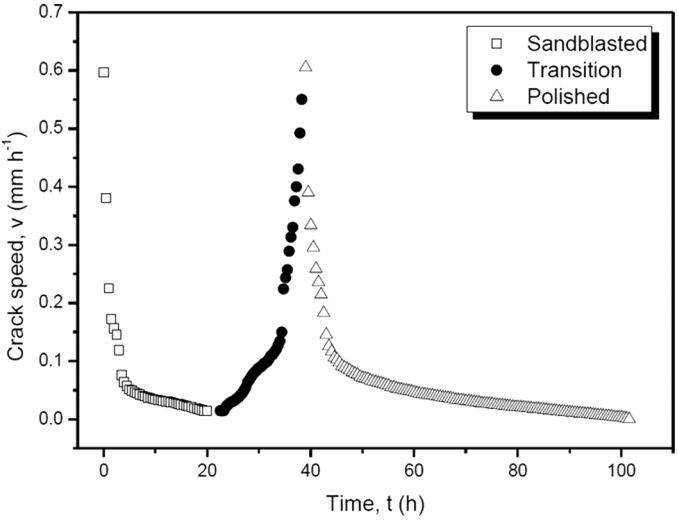

FIGURE 6 Results of Fig. 5 expressed as crack speed, da/dt, *vs.* time, t.

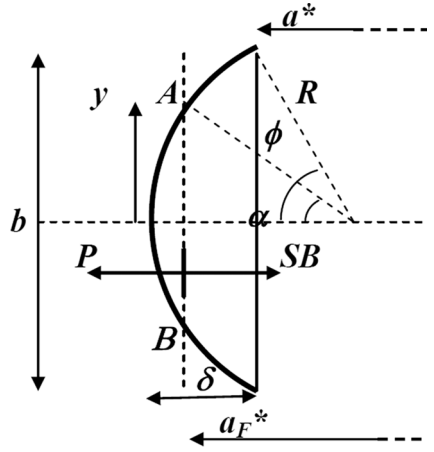

FIGURE 7 Model for curvilinear crack front traversing the frontier between *SB* and *P* treated aluminium.

decays. Clearly this "U" shape of the da/dt *vs.* t plot is related to the surface treatment transition. In order to understand the basic physics of what is occurring, we propose the following explanation.

Although the wedge test is usually considered to be two-dimensional, in fact there are some non-negligible 3D effects. In earlier work, we discussed the possible concavity of the crack front in wedge and associated adhesion fracture tests [9,23]. This phenomenon is essentially related to anticlastic curvature of the bent adherend. We therefore assume, in the present case, that the crack front is curved (convex towards the intact side of the fracture front) and may be approximated to a circular arc of low profile, such that we may write $8R\delta \approx b^2$, using the nomenclature of Fig. 7, R being the radius, δ the depth of the crack front, and b the joint width, as before. The arc subtends a (small) angle of 2ϕ. Consider the line AB, which cuts the arc in two places and represents a transition between surface treatments of the aluminium surface, sandblasting, *SB*, and polishing, *P*. We take the *SB* treatment to be on the right hand side of AB. The central part of the arc, to the left of the intersections with the line AB in the figure, subtends an angle 2α, where $0 \leq \alpha \leq \phi$. It is thus readily shown, for $\delta << b$, that to a good approximation:

$$y = \frac{b}{2}\sqrt{1 - \frac{(a_F^* - a^*)}{\delta}}; \quad (a_F^* - \delta) \leq a^* \leq a_F^*, \tag{5}$$

where a_F^* represents the distance along the x-axis between the wedge and the SB/P transition, and a^* is crack length, the asterisk denoting

that we have, arbitrarily, defined crack length as being the distance between the wedge and the fracture front taken at the joint edges. In other words, the (projected) width of the crack front on the left of AB is given by $2y = b\sqrt{1-(a_F^*-a_F)/\delta}$, with the remainder, $b(1-\sqrt{1-(a_F^*-a^*)/\delta})$, on the right of AB; thus, by hypothesis, the former is in the P zone and the latter in the SB zone.

With G_{cSB} and G_{cP} representing, respectively, fracture energy in the region pre-treated by sand-blasting and that following simple polishing, we can write an expression for the (average) fracture energy, $\overline{G}_c$, whilst the crack front finds itself cut by line AB:

$$\overline{G}_c(a^*) = G_{cSB} - \sqrt{1-\frac{(a_F^*-a^*)}{\delta}}(G_{cSB}-G_{cP}) = G_{cSB} - \sqrt{1-\frac{(a_F^*-a^*)}{\delta}}\Delta G_c, \tag{6}$$

which is a function of crack length, a^*, such that $\overline{G}_c(a^* \le (a_F^*-\delta)) = G_{cSB}$ and $\overline{G}_c(a^* \ge a_F^*) = G_{cP}$, with intermediate values of $\overline{G}_c$ for $(a_F^*-\delta) \le a^* \le a_F^*$. Generally, as the crack length, $a \approx a^*$, increases, growth rate decreases since energy release rate $G \sim a^{-4}$. However, as the crack front encroaches on the zone of simple, polished surface treatment, the intrinsic fracture energy decreases, since $G_{cP} < G_{cSB}$, such that for a given value of energy release rate G, crack speed should increase, other things being equal. Thus, there are two antagonistic effects, both being exacerbated by increasing a. If the decrease in intrinsic $\overline{G}_c$ is more significant than the effect of increased crack length, the crack will *accelerate*, contrary to the behaviour of classic wedge tests, which decelerate due to diminishing G. Thus, a graph of crack length, a, *vs.* time, t, will change from concavity towards the time axis to convexity, and the junction of the concave and convex sections of the curve, at an inflexion point where $d^2a/dt^2 = 0$ or possibly at an abrupt change of gradient $(d^2a/dt^2 = \infty)$[1], corresponds to $a^* = (a_F^*-\delta)$.

Assuming that δ remains a constant (although this is unsure at present[1]), when $a^* = a_F^*$, the crack front is *just* totally on the polished surface. Henceforth, $\overline{G}_c$ is no longer a "mixture" of G_{cSB} and G_{cP}, albeit smaller, and simply equals G_{cP}. Thus, crack growth rate will again *decrease* monotonically. Again, an inflexion point may be expected. From these two inflexions on the graph of a *vs.* t, it should thus be possible to estimate the depth of the curved crack front, δ.

[1]A short discussion on the local behaviour of the a *vs.* t relation is given in the Appendix.

If the crack front negotiates a transition from bonding on the polished treatment, P, to that on the sandblasted treatment, SB, one may expect a similar effect. However, unfortunately, the added effect of fracture on the sandblasted surface, thus leading to higher $\overline{G}_c$, will only decrease the crack growth rate even further than that due uniquely to increasing a, *viz.* $G \sim a^{-4}$. Thus, at best, one may expect a slight reduction in da/dt, but no change in overall features of the curve from concavity to convexity.

Returning to Figs. 5 and 6, we can see that the scenario described above and the scheme of Fig. 7 can explain the observed features of crack speed, da/dt, *vs.* time, t. Estimation of the positions of the inflexions in Fig. 5 leads to two corresponding values of a, and by difference, we estimate the crack depth, δ, to be $ca.$ 2.3 mm. (Note that we cannot reasonably estimate an error on δ, since the error bars correspond to position and not to gradient.) The value of 2.3 mm is quite plausible and entirely consistent with values found earlier on a similar system [9]. Further work on a system with a transparent adherend is envisaged, in order to corroborate this effect, although Fig. 4 of Reference [9] already lends credibility. However, the system will necessarily be different due to (at least one) different surface treatment, and so this will be treated as a separate study.

Fracture Energy Assessment

The data of Fig. 5 have been used to calculate the fracture energy, $\overline{G}_c$, of the aluminium/composite assembly in the vicinity of the surface treatment transition, where no distinction is made as to whether this quantity is "pure" G_{cSB} or G_{cP}, or whether Eq. (6) is applicable. This has been done using the now standard equation for fracture energy, obtained from an asymmetric wedge test, in which one adherend may be considered to be rigid [9], *viz.*:

$$\overline{G}_c = \frac{3E_C\Delta^2h^3}{8a^4}, \tag{7}$$

where E_C is Young's modulus of the composite (flexible) material (50 ± 5 GPa), other symbols having their previous meanings.

The evolution of $\overline{G}_c$ *vs.* time, t, is shown in Fig. 8. As in Fig. 5, the two representative error bars at 0 and 100 hours correspond to estimates of *systematic* errors on a, obtained using propagation of errors theory, as described in Reference [11], errors being assumed potentially to exist on E_C, Δ, h, and a. Also, as before, *relative* errors, neglecting possible misestimates of E_C, Δ, and h are far smaller, and would be difficult to discern in the figure. Figure 8 shows anticipated

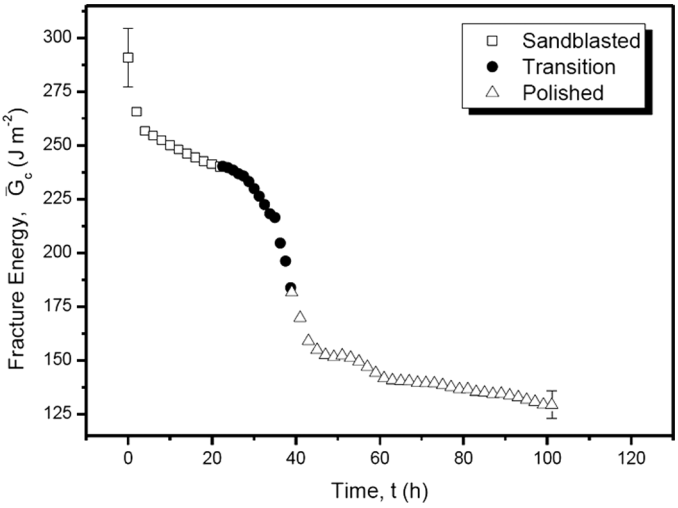

FIGURE 8 Fracture energy, $\overline{G}_c$, *vs.* time, t, in the vicinity of the transition zone.

behaviour: a decrease of $\overline{G}_c$ with time as G diminishes with crack growth, followed by a steeper decrease as the crack transfers from the *SB*-to the *P*-treated aluminium surface. Finally, a further decrease with time occurs, but at much lower values of $\overline{G}_c$ and at a lower rate of change, because the crack front is entirely in the *P* region.

Figure 9 represents fracture data in the more conventional manner, *viz.* $\overline{G}_c$ *vs.* crack speed, $v = da/dt$. The data at the top and at the bottom (accentuated by solid lines in the figure) follow the expected monotonic increase, which is well known for polymeric adhesives [24,25]. However, at first sight, this portrayal is surprising, since $\overline{G}_c$ appears to be three-valued in places. Indeed it is! The upper curve, or maximal fracture energy for a given fracture rate, may be interpreted as the fracture energy, $\overline{G}_c = G_{cSB}$, and corresponds to fracture purely in the *SB* region. Similarly, the lower curve is attributable to failure in the *P* zone, where $\overline{G}_c = G_{cP}$ (minimal energy). The data points in the intermediate region apparently indicate a *decrease* in fracture energy with increasing crack speed, which is highly unlikely under the present conditions of stable crack growth. In fact, each data point in this region corresponds effectively to a *different type of assembly*. The reason for this is that at each point, the relative contribution from each of G_{cSB} and G_{cP} is different, as given by Eq. (6) (or possibly a more accurate version thereof). Since the G_{cSB} and G_{cP} curves appear reasonably parallel, it is reasonable to suppose that, through each point,

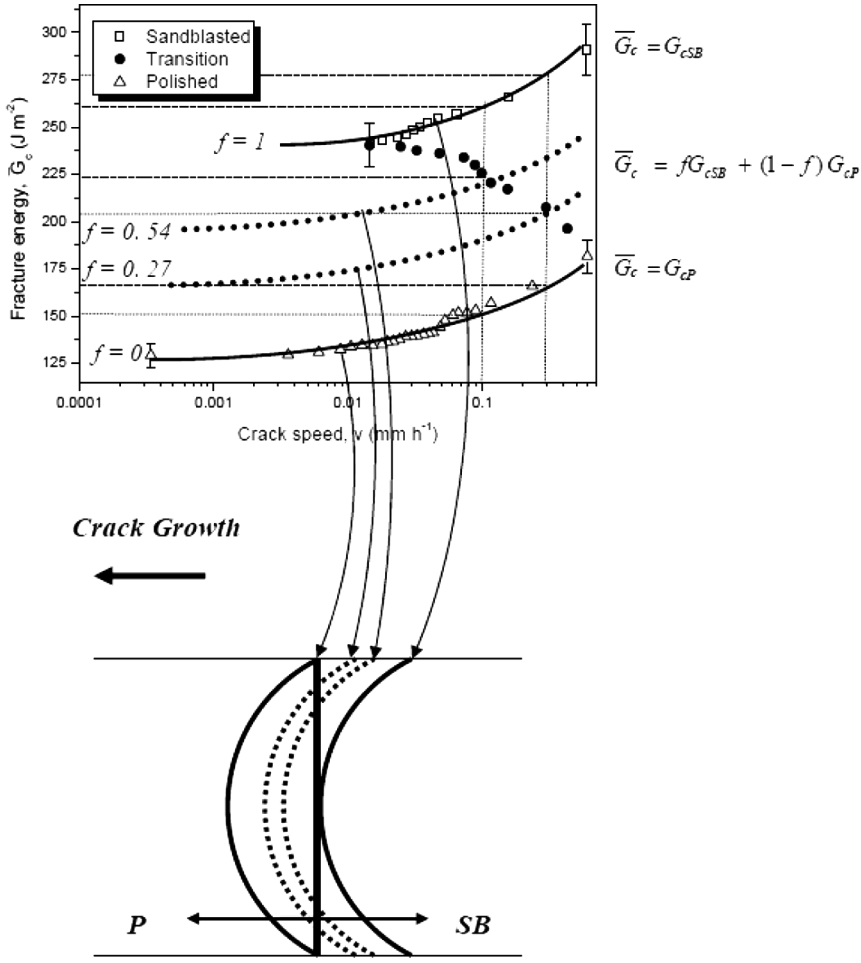

FIGURE 9 Fracture energy, $\overline{G}_c$, *vs.* crack speed, $v = da/dt$, in the vicinity of the transition zone. For $\overline{G}_c = G_{cSB}, f = 1$ and for $\overline{G}_c = G_{cP}, f = 0$. The intermediate cases (examples) correspond to $f = 0.54$ and 0.27, as shown schematically below.

we should be able to pass a curve parallel to the maximal and minimal curves. This has been done in Fig. 9 for two cases to demonstrate the principle (heavy dotted lines). To clarify the situation, we may write Eq. (6) in a simpler form as:

$$\overline{G}_c(f) = fG_{cSB} + (1-f)G_{cP}, \tag{8}$$

where f represents the fraction of surface (failure front) SB involved in the separation, and therefore $(1-f)$ corresponds to the fraction of P. Let us consider (arbitrarily) the crack speed of $v = 0.1\,\text{mm/h}$. As shown by the (light) dotted lines on the graph in Fig. 9, this corresponds to values of G_{cSB} and G_{cP}, respectively, of *ca.* 265 and $152\,\text{J m}^{-2}$. The equivalent experimental value of $\overline{G}_c$ for $v = 0.1\,\text{mm/h}$, corresponding to the intermediate case, in the transition zone, and also shown with a dotted line, is equal to *ca.* $225\,\text{J m}^{-2}$. Alternatively, we may take the known value of joint width, b, the estimated value of crack front depth, δ (see above), and together with Eqs. (6) and (8) and a knowledge of crack position, estimate f (=*ca.* 0.54). Accepting the experimental values G_{cSB} and G_{cP} above, Eq. (8) predicts a value of the intermediate $\overline{G}_c$ of *ca.* $215\,\text{J m}^{-2}$. The procedure may be repeated for a crack speed, v, of 0.3 mm/h. We find experimental and predicted values of $\overline{G}_c$, respectively, of 205 and $200\,\text{J m}^{-2}$ (f = *ca.* 0.27). (The relative data are also indicated by dotted lines in Fig. 9.) Given the simplicity of the model for crack front shape, the agreement is really quite acceptable.

Thus, the paradoxical multi-valued fracture energy curves may be explained. Clearly the model leading to Eq. (6) has its limitations (see Appendix), but the physical reason for the relatively smooth transition between types of fracture behaviour occurring on what amounts to a step function in surface treatment can be successfully explained.

CONCLUSIONS

A strain gauge technique developed for the accurate and continuous assessment of crack length in wedge tests for structural bonding, and, therefore, a more precise appreciation of fracture energy, has been applied to an aluminium alloy/epoxy composite assembly. However, we have applied two surface treatments to the aluminium alloy of each adherend, thus permitting differences in adhesion properties to be considered. A simple polishing/abrading pre-treatment led to weaker adhesion than sandblasting, as may be expected. Failure was (apparently) interfacial adhesive/aluminium for the former, whereas fracture took place near the composite/adhesive transition for the latter.

More significant in the study is the cracking behaviour when the fracture front is near the division between the two surface pretreatments. The division being a clear-cut straight line traversing the sample, a rapid change in crack growth rate, and, therefore, fracture energy, may be expected. However, a gradual transition of fracture behaviour was found, which can be successfully explained by the existence of a *curved* crack front, partially on each surface pretreatment during the transition. Also related to the curved crack front

was the discovery of a multi-valued relation between fracture energy and crack speed. This was explained by the fact that, in fact, several different systems are represented on a given set of data.

REFERENCES

[1] Ripling, E. J., Mostovoy, S., and Patrick, R. L., *Mater. Res. Standards (ASTM Bulletin)* **4**, 129–134 (1964).
[2] Mostovoy, S. and Ripling, E. J., *J. Appl. Polym. Sci.* **10**, 1351–1371 (1966).
[3] Wiederhorn, S. M., Shorb, A. M., and Moses, R. L., *J. Appl. Mech.* **39**, 1569–1572 (1968).
[4] Whitney, J. M., *Comp. Sci. Tech.* **23**, 201–219 (1985).
[5] Jethwa, J. K. and Kinloch, A. J., *J. Adhesion* **61**, 71–95 (1997).
[6] Meiller, M., Roche, A. A., and Sautereau, H., *J. Adhesion Sci. Tech.* **13**, 773–788 (1999).
[7] Sener, J. Y., Ferracin, T., Caussin, L., and Delannay, F., *Int. J. Adhesion Adhesives* **22**, 129–137 (2002).
[8] Kanninen, M. F., *Int. J. Fracture* **9**, 83–92 (1973).
[9] Popineau, S., Gautier, B., Slangen, P., and Shanahan, M. E. R., *J. Adhesion* **80**, 1173–1194 (2004).
[10] Sargent, J. P., *Int. J. Adhesion Adhesives* **25**, 247–256 (2005).
[11] Budzik, M., Jumel, J., Imielińska, K., and Shanahan, M. E. R., *Int. J. Adhesion Adhesives* **29**, 694–701 (2009).
[12] Zhang, Z. and Shang, J. K., *J. Adhesion* **49**, 23–36 (1995).
[13] Curley, A. J., Hadavinia, H., Kinloch, A. J., and Taylor, A. C., *Int. J. Fracture* **103**, 41–69 (2000).
[14] Crocombe, A. D., Ong, C. Y., and Abdel-Wahab, M. M., *J. Adhesion* **78**, 745–776 (2002).
[15] Hadavinia, H., Kinloch, A. J., Little, M. S. G., and Taylor, A. C., *Int. J. Adhesion Adhesives* **23**, 449–461 (2003).
[16] Destrebecq, J. F., Grediac, M., and Sierra-Ruiz, V., *Compo. Sci. Tech.* **67**, 707–719 (2007).
[17] Gacoin, A., Objois, A., Assih, J., and Delmas, Y., *J. Adhesion* **84**, 37–59 (2008).
[18] Bikerman, J. J., *The Science of Adhesive Joints* 2nd ed., (Academic Press, New York, 1968).
[19] Sharpe, L. H., *J.Adhesion* **4**, 51–64 (1972).
[20] Maguire, J. F., Talley, P. L., and Lupkowski, M., *J. Adhesion* **45**, 269–290 (1994).
[21] Williams, J. G., *J. Adhesion* **41**, 225–239 (1993).
[22] Cotterell, B., Hbaieb, K., Williams, J. G., Hadavinia, H., and Tropsa, V., *Mech. Mater.* **38**, 571–584 (2006).
[23] Jumel, J. and Shanahan, M. E. R., *J. Adhesion* **84**, 788–804 (2008).
[24] Gent, A. N. and Petrich, R. P., *Proc. Roy. Soc. (London)* **A310**, 433–448 (1969).
[25] Maugis, D. and Barquins, M., *J. Phys. D* **11**, 1989–2033 (1978).

APPENDIX

Behaviour of Crack Front Near *SB*/*P* Transition

We wish to consider the behaviour of crack length, a, *vs.* time, t, near the transition zone separating *SB* and *P* surface treatments on the aluminium surface prior to bonding. We assume the validity of

Eq. (6), describing the effective, or mean overall, fracture energy, $\overline{G}_c$, when the (sharp, linear) transition of surface treatment traverses the curved fracture front of Fig. 7:

$$\overline{G}_c(a^*) = G_{cSB} - \sqrt{\frac{1-(a_F^*-a^*)}{\delta}}(G_{cSB}-G_{cP}) = G_{cSB} - \sqrt{1-\frac{(a_F^*-a^*)}{\delta}}\Delta G_c. \tag{6}$$

Fracture occurs when the strain energy release rate, G, is equal to $\overline{G}_c$, and the basic relation for fracture is given by:

$$\overline{G}_c - G = \overline{G}_c + \frac{1}{b}\frac{\partial U}{\partial a} = 0, \tag{A.1}$$

where U represents stored elastic energy, b is sample width, and a is crack length. In the asymmetric wedge test, $\overline{G}_c$ is given by Eq. (7), which we write as $\overline{G}_c = ka^{-4}$, where $k = 3E_C\Delta^2 h^3/8$, since it is only variations of a that are presently of interest.

From Eqs. (6) and (A.1), we may write the threshold for fracture as:

$$G_{cSB} - \sqrt{1-\frac{(a_F^*-a^*)}{\delta}}(G_{cSB}-G_{cP}) = \frac{k}{a^4}. \tag{A.2}$$

Since the analysis leading to Eq. (7) is based on 2D analysis, it does not allow for any crack front curvature, which amounts to variability of $a = a(y)$ (see Fig. 7), and there is, therefore, some doubt as to what value of a should be used, although a^* has previously been defined as the crack length at the joint edge. Notwithstanding this detail for the moment, Eq. (A.1) is differentiated with respect to time, t, and arranged to give:

$$\frac{d^2a}{dt^2}\left\{\frac{dG_{cSB}}{dv}\left[1-\left(1-\frac{(a_F^*-a^*)}{\delta}\right)^{1/2}\right]+\frac{dG_{cP}}{dv}\left(1-\frac{(a_F^*-a^*)}{\delta}\right)^{1/2}\right\}$$
$$=\frac{(G_{cSB}-G_{cP})v}{2\delta}\left[1-\frac{(a_F^*-a^*)}{\delta}\right]^{-1/2}-\frac{4kv}{a^5}, \tag{A.3}$$

where $v = da^*/dt = da/dt$, assuming that it is permissible to equate the two derivatives (an additive constant between them). For the moment, we take it that δ is constant.

Now when the crack front first reaches the SB/P transition, $a^* = (a_F^* - \delta)$ (see section "Crack Length and Fracture Energy" and Fig. 7). Evaluation of Eq. (A.3) at this point leads to:

$$\frac{d^2a}{dt^2}\frac{dG_{cSB}}{dv} = \frac{(G_{cSB}-G_{cP})}{2\delta}\frac{v}{0}-\frac{4kv}{a^5}. \tag{A.4}$$

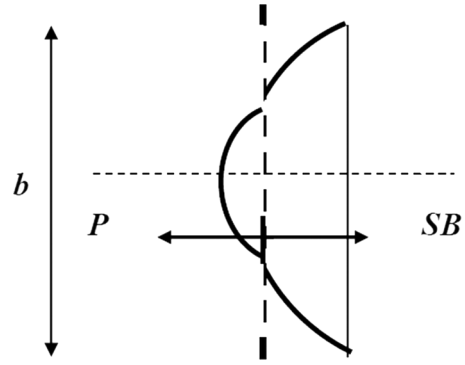

FIGURE A1 Suggested sketch of crack front "bubbling" as it encounters the sharp transition between *SB* and *P* treated aluminium.

Thus, since k, v, and a are finite and positive, provided $G_{cSB} > G_{cP}$, and $dG_{cSB}/dv > 0$, which is clearly the case, $d^2a/dt^2 = \infty$. The experimental data suggest strongly an inflexion point, corresponding to $d^2a/dt^2 = 0$, rather than a sharp change in da/dt ($d^2a/dt^2 = \infty$). This, in turn, suggests that δ varies (if only slightly) as the SB/P frontier is encroached upon, since this will permit the denominator of the first term on the right hand side of Eq. (A.4), *i.e.,* the term in $(1 - (a_F^* - a^*)/\delta)^{-1/2}$ in Eq. (A.3), to remain finite. Clearly δ cannot decrease, or contact with the transition will be lost, and so δ must increase. From a purely intuitive, physical point of view, this also seems reasonable, since adhesion is less good in the P region, and with a similar local moment, or value of G, the anticlastic effect is likely to become exacerbated, increasing δ. A sketch of the expected scenario is given in Fig. A.1. As the crack front encroaches onto the zone of lower adhesion, separation occurs more readily, leading to a "bubble"-like failure area.

The same consideration can be given to the case, occurring later, when the entire crack front is *just* on the P region, *i.e.,* when $a^* = a_F^*$, but simple substitution into Eq. (A.4) reveals that this situation leaves d^2a/dt^2 finite (and possibly 0) under expected conditions.